INSTITUTE OF PHYSICS PUBLISHING PLASMA PHYSICS AND CONTROLLED FUSION

Plasma Phys. Control. Fusion **46** (2004) A95–A104 PII: S0741-3335(04)70278-X

Local threshold conditions and fast transition dynamics of the L–H transition in Alcator C-Mod

A E Hubbard[1,4], B A Carreras[2], N P Basse[1], D del-Castillo-Negrete[2], J W Hughes[1], A Lynn[3], E S Marmar[1], D Mossessian[1], P Phillips[3] and S Wukitch[1]

[1] MIT Plasma Science and Fusion Center, Cambridge, MA 02139, USA
[2] Oak Ridge National Laboratory, Oak Ridge, TN 37831, USA
[3] Fusion Research Center, University Texas at Austin, TX 78712, USA

E-mail: Hubbard@psfc.mit.edu

Received 10 October 2003
Published 5 April 2004
Online at stacks.iop.org/PPCF/46/A95
DOI: 10.1088/0741-3335/46/5A/010

Abstract

Edge profiles during the L–H transition and pedestal evolution in the Alcator C-Mod tokamak have been measured with high spatial and time resolution. For input power near the threshold, periodic 'dithering' cycles are seen, and the sustained transition occurs in a series of steps that appear related to this oscillatory behaviour. Even at a higher power, there is evidence of non-smooth T_e evolution, and the pedestal T_e shows a double break-in-slope at the transition. Calculations with a fluctuation-shear flow model, for parameters typical of this experiment, reproduce much of the observed behaviour. Profiles just before the L–H transition, averaged over steady or dithering periods, are compared with an analytic criterion based on shear suppression by zonal flows (Guzdar P N *et al* 2002 *Phys. Rev. Lett.* **89** 265004). The experimental values of $T_e/\sqrt{L_n}$ are about 50% below the theoretical threshold, for a range of B_T.

1. Introduction

The spontaneous transition from the low confinement mode (L-mode) to the high confinement mode (H-mode), characterized by a decrease in turbulence and in particle and energy transport near the last closed flux surface (LCFS), is widely observed in many tokamaks and other magnetic confinement devices [1]. However, its understanding is far from complete. There is general consensus that transport is suppressed by $E \times B$ shear flow. Many terms can be involved in such shear, including mean poloidal or toroidal flows (V_θ, V_ϕ), diamagnetic terms due to ∇p, and rapidly fluctuating, turbulence-generated, 'zonal' flows, all of which are potentially important in the feedback loop leading to suppression. Part of the ongoing difficulty in determining the details of the transition mechanism is that many terms are hard to

[4] Author to whom any correspondence should be addressed.

measure with sufficiently high spatial and temporal resolution over the edge region of interest; parameters can vary by an order of magnitude over a few millimetres and on sub-millisecond timescales. Improvements in diagnostics thus lead to more detailed knowledge about the conditions for, and dynamics of, the L–H transition. This paper documents the most recent measurements of the transition on the Alcator C-Mod tokamak and makes comparisons with some available theoretical models.

Prior studies of the L–H threshold on C-Mod focused on the local plasma parameters in the edge plasma just before the transition. For a given magnetic configuration, the edge electron temperature, T_e, was in a narrow range at the transition for a range of densities, strongly suggesting a threshold condition in this or a closely related parameter [2]. Similar results have been reported in ASDEX Upgrade and other tokamaks [3]. At the time of these studies, T_e measurements had limited radial resolution and there was little direct information on the edge n_e profile, so that parameters involving gradients of T_e or n_e could not be evaluated accurately. Other groups, particularly the DIII-D team, have proposed alternative thresholds in ∇T or ∇p [4] and recently claimed good agreement with a threshold condition based on shear suppression by zonal flows [5]. Kaye *et al* [6], in contrast, do not find consistency with any of these thresholds in NSTX. High resolution edge Thomson scattering (ETS) in C-Mod now provides accurate profiles of both temperature and density.

Previous studies of the dynamic behaviour in C-Mod focused on the response at slow timescales as power was ramped slowly up and down, causing controlled transitions from L- to H-mode and back to L-mode [7]. Measured flux–gradient relationships showed the classic 'S-curve' as predicted by theoretical bifurcation models. Investigations of fast dynamics at the L–H transition were limited by the signal-to-noise and time resolution of T_e and n_e measurements, and results were not very reproducible. In the following section, the improved edge diagnostic set and the plasma parameters of some recent experiments designed to optimize the measurements of thresholds and dynamics are described. Section 3 gives fast measurements of the edge profile evolution, at a range of powers and showing some interesting oscillatory behaviour. Section 4 describes a model of the transition in which edge fluctuations, poloidal shear flows and pressure are evolved. Calculations for the parameters of the C-Mod experiments reproduce some of the observed behaviour. In section 5, profile measurements just before the L–H transition are compared with threshold predictions of Guzdar *et al* [5]; reasonable agreement is found. Conclusions and areas for further work are discussed in section 6.

2. Diagnostics and experimental conditions

Profiles of T_e and n_e are routinely measured by an ETS diagnostic with 1.5 mm radial resolution and 16 ms time resolution [8]. A higher time resolution is provided by electron cyclotron emission (ECE) and visible bremsstrahlung (VB) measurements. Grating polychromators have been supplemented by a 32-channel heterodyne radiometer, which can measure at up to 1 μs [9]. For these L–H studies, signals are sub-sampled at 50 μs, giving low noise levels of $\sim$5 eV. The radial resolution is $\sim$5 mm, predominantly due to flux surface averaging of the off-axis viewing optics. The density is derived from VB emissivity assuming flat $Z_{\rm eff}$ profiles. The 2048 pixel CCD array used for the VB measurement has 1 mm radial resolution and has been upgraded to 0.5 ms time resolution [10]. Because of the high density characteristic of C-Mod plasmas, we assume that $T_i \simeq T_e$.

Auxiliary heating in C-Mod is provided by up to 5 MW of ICRF heating. This has the advantage for threshold studies that the input power is rapidly and continuously variable and radially localized. In the usual central heating scenario, large sawteeth oscillations are produced

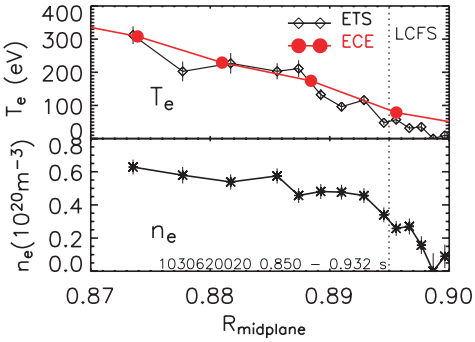

Figure 1. ETS profiles of electron temperature (top) and density (bottom) for C-Mod discharge 1030620020, with $P_{RF} = 1.4$ MW, averaged over a period of 82 ms before the L–H transition. T_e from the heterodyne ECE diagnostic is shown for comparison (●, top).

in the central T_e. The resulting heat pulses are clearly visible in $T_e(r, t)$ out to the edge and can be a complication when studying the threshold and dynamics. The power flux across the edge region is non-steady, and L–H transitions are often triggered by a heat pulse. To avoid this, dedicated experiments were carried out with off-axis ICRH at $f = 78$–80 MHz, at a toroidal field of 6.1 T and plasma current of 0.8 MA ($q_{95} = 5.4$). Centring the power deposition at $r/a = 0.5$, outside the $q = 1$ surface, reduces the size of the central sawteeth to close to their ohmic level, and heat pulses are no longer discernable at the edge. In a shot-to-shot power scan at L-mode target density $\bar{n}_e = 1.45 \times 10^{20}$ m^{-3}, RF power was turned on at $t_{RF} = 0.8$ s, reaching its full power in 10 ms.

The lowest power at which an L–H transition occurred was $P_{RF} = 1.25$ MW. As will be shown in more detail below, transitions at $P \simeq P_{thresh}$ are preceded by ∼100 ms of regular 'dithering' cycles, and a sustained pedestal does not form until up to 200 ms after t_{RF}. Edge profiles averaged over such a quasi-steady period are shown in figure 1. ECE and ETS measurements of T_e agree well, indicating that ECE is a reliable diagnostic of temperature out to R_{sep}, even though optical depth is dropping; there is no sign of non-thermal emission. Excursions in T_e during the dithering cycles are small (typically 20–30 eV, see figure 2), so that an average over these periods is within ∼10% of the L-mode value. As expected, as P_{RF} was increased, the transition occurred progressively earlier. At the highest power of 5 MW, there is only a 15 ms delay from t_{RF}, less than the energy confinement time $\tau_E \sim 40$ ms. The heat flux is thus not yet in steady state, and a careful power accounting is required. To assess the instantaneous heat flux crossing the LCFS, we use $P_{net} = P_{RF}\eta_{RF} + P_{OH} - P_{rad} - dW_{MHD}/dt$, where we take a constant ICRF heating efficiency $\eta_{RF} = 0.7$, core P_{rad} from inverted bolometry arrays, and P_{OH} and W_{MHD} from fast equilibrium reconstructions using EFIT [11]. At the transition time, dW_{MHD}/dt is up to 1.5 MW, and P_{net} varies by only 50%, from 1.4 to 2.0 MW, despite the factor of 3.5 range of RF power. This implies that the transition occurs quite promptly once the required instantaneous flux or local parameters are reached and that it is experimentally very difficult to produce L–H transitions with $P \gg P_{thresh}$. The range achieved is, however, sufficient to affect the dynamics of the transition, as shown in the following section.

3. Measurements of fast dynamics at the L–H transition

The most striking feature noted consistently in observations of profile evolution through the L–H transition is that T_e increases in two stages. There is an initial rapid increase lasting

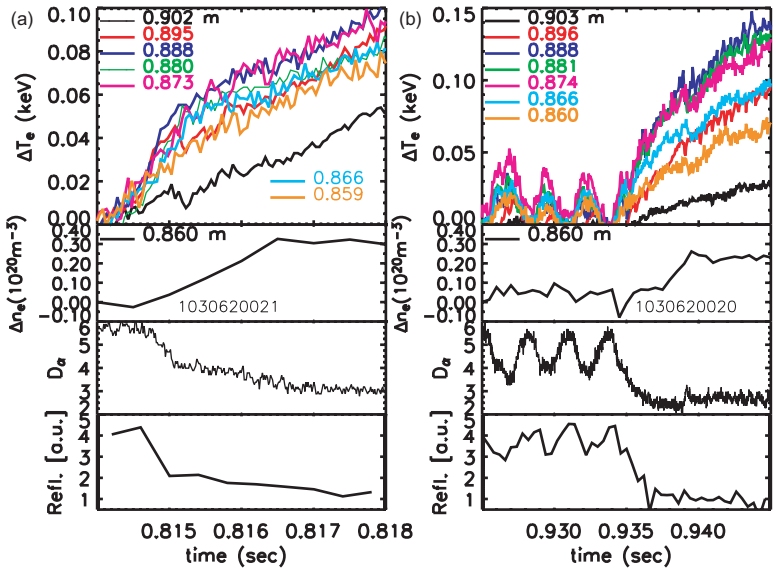

Figure 2. Time evolution near the L–H transition for two discharges in an RF power scan: (*a*) $P_{RF} = 5.0$ MW and (*b*) $P_{RF} = 1.4$ MW. Signals shown, from top to bottom are (i) changes in T_e for seven radial channels of heterodyne ECE, (ii) change in n_e at $R = 0.86$ cm, derived from VB array, (iii) D_α emission, showing drop at L–H transition, and (iv) autopower spectrum from a reflectometer channel at $f = 88$ GHz, integrated from 20 to 350 kHz. Note that a longer time window is shown for (*b*) to illustrate some of the 'dithering' cycles before the sustained transition.

$\sim$700 μs and a more gradual, apparently diffusive response as the pedestal profile evolves to its new equilibrium value over tens of milliseconds. The change in T_e is shown in figure 2(*a*) for several heterodyne ECE channels for a high power discharge. The fast increase extends for $\sim$3 cm inside the separatrix at $R_{sep} = 89.5$ cm; its amplitude typically peaks at 88–89 cm. This is wider than the eventual pedestal region, which extends to $R \cong 89.0$ cm. At smaller radii, only a single, smooth response is seen. There is also no jump apparent in the scrape-off layer (SOL), though ECE measurements are not reliable in this low density region. The gradient, ∇T_e , however, increases only between one channel pair (7 mm apart) just inside R_{sep}, approximately the region of the H-mode pedestal. Inboard of this region, ∇T_e is constant or flattens transiently. The region of increasing ∇T_e thus seems the most relevant place to study, and model, the dynamics. Also apparent in figure 2(*a*) is that, on the outer channels, there is a slight decrease in T_e at the end of the fast rise period. Analysis of bremsstrahlung profiles in the region of steep and rapidly changing T_e is complicated since emissivity depends on T_e and Z_{eff} as well as n_e. Slightly inside the pedestal, at $R = 0.86$ m, the derived n_e increases at the transition as expected, typically doubling from the L-mode to the steady H-mode. Its relative variation in the first 700 μs (the period of the fast transient) is only $\sim$15%.

More complex dynamics is seen in the lowest power transitions with power near the threshold. An example with $P_{RF} = 1.4$ MW is shown in figure 2(*b*). Repeated cycles, with period $\sim$3 ms, are seen in which D_α drops and T_e transiently rises by about 20 eV. The density inboard of the pedestal shows a slight, poorly resolved, increase. A modest decrease is seen in the density fluctuation level, as measured by a reflectometer channel at $f = 88$ GHz. T_e then drops, D_α and fluctuations increase, and the cycle repeats. The eventual, sustained, transition occurs in a series of 'steps', with T_e rising for $\sim$0.5 ms and then dropping slightly before rising further; the period of these steps is $\sim$1 ms, slightly shorter than that of the preceding limit cycles.

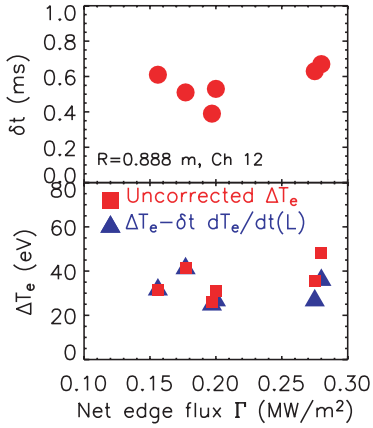

Figure 3. Scaling of the duration, δt (top), and amplitude, ΔT_e (bottom) of the fast rise phase following an L–H transition with the net power flux at the transition. Triangles represent ΔT_e after correcting for the increase that would have occurred without the transition.

To investigate more systematically the dependence of the fast transition timescale on the input power, time traces of T_e were fit for each of several discharges to a function with three linear slopes, before, during, and after the initial transient; the first break-in-slope defines the L–H transition time and the second the end of the fast rise. Where there was a subsequent decrease, the function fit the time to the start of this 'dip'. Figure 3 shows the results for the channel at 88.8 cm (7 mm inside R_{sep}), plotted against the net power flux, Γ, at the L–H transition; results for other positions were very similar. Perhaps surprisingly, there is little variation in the duration of the transient, which remains at $530 \pm 140\,\mu$s; it does not shorten, as might have been expected, at a higher flux. The change in T_e during the transient is also nearly constant, with perhaps a weak increase with power. In the high power, non-equilibrium discharges, dT_e/dt is significant even in the L-mode. After correcting for this, the power dependence of the amplitude also disappears (triangles), with all cases 'jumping' by 33 ± 8 eV. The similarity in timescales between the 'steps' in the low power cases preceded by dithering, and the fast jump seen in higher power cases strongly suggests that both are caused by the same mechanism and that turbulence and transport levels can oscillate before settling to their H-mode equilibrium value. These observations have been used to guide models of the transition.

4. Modelling of dynamics at the L–H transition

In order to gain some insight into the time behaviour of the edge profiles at the L–H transition, we apply a spatially non-local fluctuation flow model developed by Diamond *et al* [12, 13]. In the three-equation version of this model, the local poloidal flow shear, $\langle V_\theta \rangle'$, the local fluctuation intensity, $E \equiv \langle (\tilde{n}_k/n_0)^2 \rangle^{1/2}$, and the local pressure, p, evolve according to the coupled equations

$$\frac{\partial E}{\partial t} = \gamma_0 \left(-\frac{a}{p_0} \frac{\partial p}{\partial x} \right) E - \alpha_1 E^2 - \alpha_2 \langle V_E \rangle'^2 E + \frac{\partial}{\partial x} \left[(D_A E + D_0) \frac{\partial E}{\partial x} \right], \quad (4.1)$$

$$\frac{\partial \langle V_\theta \rangle'}{\partial t} = -\hat{\mu} \langle V_\theta \rangle' + \alpha_3 \langle V_E \rangle' E + \frac{\partial^2}{\partial x^2} \left[(D_A E + D_0) \langle V_\theta \rangle' \right], \quad (4.2)$$

$$\frac{\partial p}{\partial t} = S(x) + \frac{\partial}{\partial x} \left[(D_A E + D_0) \frac{\partial p}{\partial x} \right]. \quad (4.3)$$

The poloidal flow velocity is related to the $E \times B$ shear velocity, $\langle V_E \rangle$, through the radial force balance equation:

$$\langle V_\theta \rangle = \langle V_E \rangle + \frac{1}{eBn} \frac{\mathrm{d}P_\mathrm{i}}{\mathrm{d}x}.$$

For simplicity, we assume that the time dependence of the pressure is the result of a constant density and time-varying temperature. These equations and the definition and formulae used for the various parameters are discussed in detail in [12, 14]. To summarize, D_0 is the collisional diffusivity, computed from neoclassical theory, and $D_\mathrm{A}E$ is the turbulence induced one, estimated from L-mode experimental measurements. In equation (4.1),

$$\gamma \equiv \gamma_0 \left(-\frac{a}{p_0} \frac{\partial p}{\partial x} \right)$$

is the linear growth rate of the edge turbulence underlying instability in the absence of sheared flow. The second term in the right-hand side is responsible for the saturation of turbulence in the L-mode and the third is the shear suppression term. The α_2 coefficient is estimated [15] as $\alpha_2 \approx (k_\theta W)^2/\gamma_0$, where W is the radial decorrelation length of the turbulence. In equation (4.2), for poloidal flow shear, the first term in the right-hand side is the poloidal flow damping by magnetic pumping. The flow damping rate, $\hat{\mu} = \mu_{00}\nu_{ii}$, is calculated using neoclassical expressions from Hirshman and Sigmar [16]. The second term in the right-hand side is the Reynolds stress term and the third term represents diffusion. The angular bracket, $\langle\,\rangle$, indicates poloidal and toroidal averages over a magnetic flux surface. Equation (4.3) is a transport equation for the evolution of the plasma pressure. The source term is $S(x)$, and the transport coefficient is assumed to be the same as for the other equations.

The equations are normalized and solved in a radial layer at the plasma edge, where it is assumed that the heat source, $S(x)$, is zero and a constant heat flux, Γ_0, flows from the plasma core at $x = 0$, providing the boundary condition for the pressure gradient:

$$\Gamma_0 = -(D_\mathrm{A}E + D_0) \frac{\partial p}{\partial x}\bigg|_{x=0}.$$

Different stable fixed-point solutions are possible in this model, depending on this flux [17]. At low Γ_0, there is negligible shear flow and $p(x)$ is linear with a gradient set by the anomalous diffusivity. This solution corresponds to L-mode transport. Above a threshold Γ_c, the shear flow increases and fluctuations saturate or decrease slightly. At still higher flux, the fluctuations are quenched by flows and a higher linear gradient is set by neoclassical transport. This solution corresponds to the H-mode, and it is this higher threshold, $\Gamma_{\mathrm{c,eff}}$, that would be seen in experiment as the L–H threshold flux.

To study the transition dynamics, the system of equations (4.1)–(4.3) is solved using a finite difference representation on an equal-spaced radial grid and using an explicit time evolution scheme. The dynamic behaviour has been shown to vary depending on the parameters used, particularly the ratios of α_1, α_2 and α_3. For model calculations of the transition for the C-Mod experiment, we take plasma parameters from measured profiles near the transition (e.g. figure 1). At $R = 88\,\mathrm{cm}$, just inboard of the top of the pedestal, $T_\mathrm{e} = 250\,\mathrm{eV}$, $n_\mathrm{e} = 6 \times 10^{19}\,\mathrm{m}^{-3}$, and $L_\mathrm{p} = 3\,\mathrm{cm}$. We take the plasma edge turbulent diffusivity to be $D_\mathrm{A}E \sim 10^4\,\mathrm{cm}^2\,\mathrm{s}^{-1}$ based on an edge power balance analysis assuming equal conduction by electron and ion channels. The fluctuation level, $\tilde{n}/n$, is estimated to be 10%, giving transport consistent with this diffusivity. This seems reasonable since probe measurements in the SOL typically show $\tilde{n}/n \sim$ 30–50%, and fluctuations are expected to decrease inside the LCFS. These parameters correspond to $\alpha_1 = 6.25 \times 10^5\,\mathrm{s}^{-1}$, $\alpha_3 = 3.47 \times 10^5\,\mathrm{s}^{-1}$, $\gamma_0 = 2.5 \times 10^4$, $W = 0.13\,\mathrm{cm}$, and $a_3 \equiv \alpha_3/\alpha_1 = 0.55$. Other estimates of $D_\mathrm{A}E$ using the mixing length

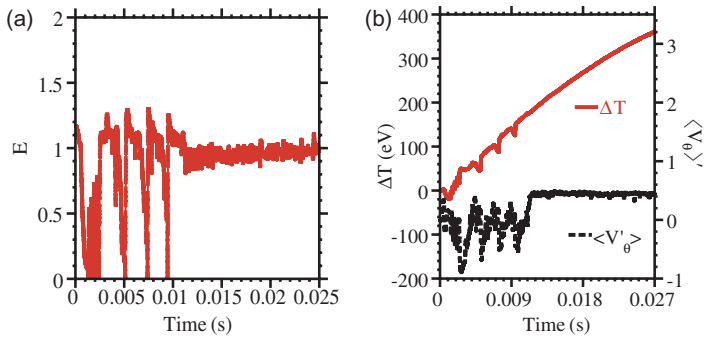

Figure 4. Model calculations of the L–H transition for C-Mod parameters. (*a*) Normalized fluctuation amplitude, E. (*b*) Flow shear, $\langle V_\theta \rangle'$ (dashed black line), and change in T_e (solid red line). The oscillations in E and $\langle V_\theta \rangle'$ lead to stepwise increases in ΔT_e.

approximation and assuming drift-wave turbulence gave unrealistically low turbulence and diffusion levels.

Initial simulations were run assuming $\langle V_E \rangle = \langle V_\theta \rangle$, i.e. neglecting the diamagnetic contribution. In this case, fluctuations were quenched in $\sim$200 μs and there was a smooth evolution of the edge pressure; this is characteristic of solutions where $a_3 < 1$. With diamagnetic terms included and flux of $\Gamma_0 = 0.33\,\mathrm{MW\,m^{-2}}$, within 10% of $\Gamma_{c,\mathrm{eff}}$, more complex behaviour is seen (as shown in figure 4). The fluctuation levels and flows exhibit several cycles of suppression and regrowth to their L-mode levels, with a period of 2–3 ms. The temperature, T, responds, increasing during the period of low fluctuation amplitude and then decreasing slightly as the turbulence increases. Its evolution is similar to that seen in the experiment at flux close to the L–H threshold (as shown in figure 2(*b*)). In other calculations at higher fluxes up to twice $\Gamma_{c,\mathrm{eff}}$ (which is a larger range than achieved in experiment), the T_e oscillations during the transition become higher in frequency and much smaller in amplitude; they would likely not be observable. It should be noted that these calculations do not separately evolve the density and temperature. Increases in n_e during each period of fluctuation decrease would be expected to cause a stronger 'dip' in T_e, perhaps even leading to the periodic return to L-mode values seen in the pre-transition 'dithering' cycles. For the parameters used, we have not seen in these calculations the 'two phase' evolution of T_e that was seen experimentally at radii near the top of the pedestal in higher power cases. It should be noted that the present model does not incorporate many of the detailed features of the experiment. It is expected to give only a limited description of the transition phenomena with the right order of magnitude for the different scales.

5. Edge profiles at the L–H threshold and comparison with theoretical predictions

Discharges with long periods of constant input power and near-steady plasma conditions just before an L–H transition are ideal for assessment of local threshold conditions necessary for confinement bifurcation. ETS profiles can be averaged over multiple laser pulses, leading to low statistical errors as shown in figure 1. This then allows local gradients and scale lengths, such as ∇n_e and $L_n \equiv n_e/\nabla n_e$, to be computed accurately. Such quantities appear in several theoretically predicted thresholds. As an initial application of this technique, we compare C-Mod profiles with the recently published threshold criterion of Guzdar *et al* [5]. This is based on the shear suppression of resistive turbulence by self-generated zonal flows, as was

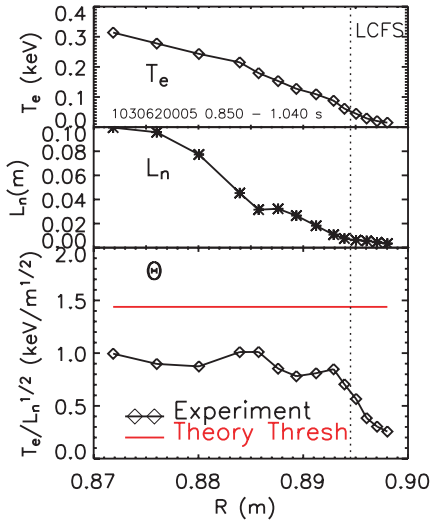

Figure 5. Evaluation of threshold parameters at the L–H transition for a 6.1 T discharge. T_e (top) and L_n (middle) are measured from ETS and used to compute $\Theta \equiv T_e/\sqrt{L_n}$ (bottom). The horizontal line represents the theoretical threshold, Θ_c.

found in simulations by Rogers *et al* [18]. The analytic criterion is based on the finding that the growth rate for the generation of zonal flows by finite beta drift waves has a minimum at a critical $\hat{\beta}$, where $\hat{\beta} \equiv \beta(qR/L_n)^2/2$ [19]. It has the attraction for experimental comparison that it leads to a simple and readily evaluated condition for the transition:

$$\Theta \equiv \frac{T_e}{\sqrt{L_n}} = 0.45 \frac{B_T(T)^{2/3} Z_{eff}^{1/3}}{[R(m)A_i]^{1/6}}. \tag{5.1}$$

Here, A_i is the atomic mass and Z_{eff} the effective charge. This criterion was found to correspond well to DIII-D profiles in a variety of plasma conditions [5]. The C-Mod data offer the opportunity to check it at a higher field and smaller major radius.

For consistency with the DIII-D evaluation, we evaluate Θ_c using R and the magnetic field on axis, and assuming $Z_{eff} = 1$. Since it is not clear *a priori* where Θ will be maximized and, presumably, the transition triggered in this theory, we evaluate across the edge region and look for its largest value, Θ_{max}. Figure 5 shows radial profiles of T_e and L_n from ETS for a discharge similar to that of figure 1 but with an even longer dithering period. Three-point radial smoothing has been applied to reduce non-physical structure due to small channel-to-channel uncertainties in calibration. Since both quantities increase with distance inside R_{sep}, Θ in fact has a nearly flat profile in the region 88.4–89.3 m. The horizontal line represents the predicted threshold, Θ_c, computed according to equation (5.1). It can be seen that the experimental Θ_{max}, 0.8–1.0 in the region of interest, is about 50% below the predicted value of 1.44 at this B_T. Given the simplicity of this analytical model and the fact that no numerical parameters were adjusted from the DIII-D comparisons, this seems quite good, though not perfect, agreement. It should be noted if instead Θ_c is evaluated at the outer midplane ($R = 0.89$ m), Θ_c would be reduced systematically by 22%, to 1.12 in this case. On the other hand, using the experimental Z_{eff} (typically 1.8) would raise Θ_c by about the same amount. The model is being extended to include T_i effects, which may in fact reduce the predicted threshold and give better agreement with the data [20].

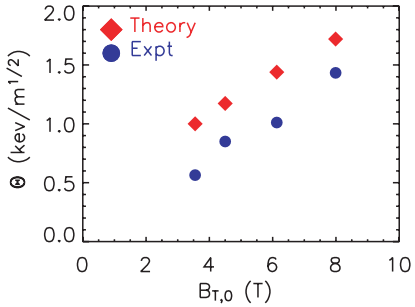

Figure 6. Experimental (●) and theoretical (♦) values of $\Theta \equiv T_e/\sqrt{L_n}$ vs toroidal field.

The dedicated experiment described in section 2 was at a fixed target density and field, and all discharges with power close to the threshold had edge profiles very similar to the one shown. In H-mode, since T_e rises and L_n decreases in the pedestal, Θ_{max} increases to 1.9–3.5 depending on power, well above Θ_c. In the ohmic L-mode period before RF was applied, L_n is similar to that at the threshold, but edge T_e is ∼30% lower inboard of R_{sep}. Θ reaches its maximum value of 0.65 just inside R_{sep}. The rather flat profiles of $\Theta(r)$ leave open the question of where exactly the transition is initiated and what sets the eventual pedestal width. Since Θ varies little with RF power at the LCFS, which is to be expected, given SOL power balance considerations, a point further inboard seems more likely in this theory.

A few discharges were identified from other, non-dedicated experiments with toroidal fields varying from 3.5 T (ohmic H-mode) to 8 T (D–He^3 ICRF), which also had long steady or dithering periods. The results are summarized in figure 6. $\Theta(r)$ was evaluated as above and generally exhibits a local maximum ∼5 mm inside R_{sep}. Θ_{max} (circles) scales with B_T approximately as predicted by equation (5.1), remaining about 50% below the predicted threshold value (diamonds).

6. Conclusions and further work

The addition of edge profile diagnostics with higher spatial and temporal resolution and experiments with well controlled input power have enabled more detailed study of the L–H transition and pedestal evolution on C-Mod. Near the threshold, periodic 'dithering' cycles are seen, and the sustained transition occurs in a series of 'steps' that may well be related to the oscillatory behaviour. Even at a higher power, there is evidence of non-smooth T_e evolution, particularly near the separatrix; near the top of the pedestal, T_e shows a double break-in-slope at the transition. We have shown that a fluctuation-shear flow model can, for parameters typical of the experiment, reproduce much of the observed behaviour. It should be pointed out that such oscillatory limit cycles are not unique to this model; other L–H transition models, e.g. [21], have also exhibited this under certain conditions. A recent paper by Kim and Diamond [22] suggests that the presence of zonal flows can modify the dynamics and perhaps extend the oscillatory period. It may not be possible to distinguish unambiguously between the effects of mean and fluctuating flows without measuring them; diagnostic development is under way to attempt this. Complete modelling of the pedestal formation will require separate evolution of the density and temperature.

Analysis of profiles just before the L–H transition, averaged over steady or dithering periods, shows quite good agreement with an analytical criterion based on shear suppression by zonal flows. The experimental values of $T_e/\sqrt{L_n}$ are about 50% below the theoretical

threshold, for a range of B_T. The limited number of discharges analysed to date all had quite similar profiles of L_n. It is thus not possible on the basis of these C-Mod data to distinguish between a threshold in T_e, as previously reported, and one in $T_e/\sqrt{L_n}$. However, Guzdar's theory [5] appears a possible candidate on the basis of these initial comparisons, as well as those in DIII-D, and the averaging technique has proven to be useful. The different threshold behaviour reported in NSTX to that on other tokamaks remains to be explained and might indicate aspect ratio or fast ion effects [6]. It is planned in the next C-Mod campaign to conduct further threshold experiments in a wider range of conditions, including upper and double null plasmas and a range of densities, which might be expected to vary L_n and provide a stronger test of theories as well as improve statistics. These experiments, and comparisons with other theories, will be reported in a future publication.

Acknowledgments

We wish to thank P Guzdar, University of Maryland, for his advice on evaluating threshold parameters for model comparison, and P Diamond (UCSD) for useful discussions on pedestal evolution. This work was supported by US Department of Energy Contracts DE-FC02-99ER54512, DE-FG03-96ER54373, and DE-AC05-00OR22725.

References

[1] Burrell K H 1997 *Phys. Plasmas* **4** 1499–518
[2] Hubbard A E *et al* 1998 *Plasma Phys. Control. Fusion* **40** 689–92
[3] Suttrop W *et al* 1997 *Plasma Phys. Control. Fusion* **39** 2051–66
[4] Groebner R J, Thomas D M and Deranian R D 2001 *Phys. Plasmas* **8** 2722
[5] Guzdar P N, Kleva R G, Groebner R J and Gohil P 2002 *Phys. Rev. Lett.* **89** 265004
[6] Kaye S M *et al* 2003 *Phys. Plasmas* **10** 3958
[7] Hubbard A E *et al* 2002 *Plasma Phys. Control. Fusion* **44** A359–66
[8] Hughes J W *et al* 2001 *Rev. Sci. Instrum.* **72** 1107
[9] Chatterjee R *et al* 2001 *Fusion Eng. Des.* **53** 113
[10] Marmar E S *et al* 2001 *Rev. Sci. Instrum.* **72** 940
[11] Lao L L and Jensen T 1991 *Nucl. Fusion* **31** 1909
[12] Diamond P H, Lebedev V B, Newman D E and Carreras B A 1995 *Phys. Plasmas* **2** 3685
[13] Diamond P H, Liang Y-M, Carreras B A and Terry P W 1994 *Phys. Rev. Lett.* **72** 2565
[14] del-Castillo-Negrete D, Carreras B A and Lynch V E 2004 *Plasma Phys. Control. Fusion* **46** A105
[15] Biglari H, Diamond P H and Terry P W 1990 *Phys. Fluids* B **2** 1
[16] Hirshman S and Sigmar D J 1981 *Nucl. Fusion* **21** 1079
[17] Carreras B, Newman D, Diamond P H and Liang Y-M 1994 *Phys. Plasmas* **1** 4014
[18] Rogers B *et al* 1998 *Phys Rev. Lett*. **81** 4396
[19] Guzdar P N *et al* 2001 *Phys. Rev. Lett*. **87** 15001
[20] Guzdar P N 2003 private communication
[21] Itoh S-I and Itoh K 1991 *Phys. Rev. Lett.* **67** 2485
[22] Kim E and Diamond P D 2003 *Phys. Rev. Lett*. **90** 118